Sedimentation and sediment geochemistry in a tropical mangrove channel meander, Sungai Kerteh, Peninsular Malaysia

Hasrizal Bin Shaari (riz@umt.edu.my)
Universiti Malaysia Terengganu https://orcid.org/0000-0002-7738-3885
Qatrunnada Mohd Nasir
Universiti Malaysia Terengganu
Che Abd Rahim Mohamed
Universiti Kebangsaan Malaysia
Abdul Hafidz Yusoff
Universiti Malaysia Kelantan
Wan Mohd Afiq Wan Mohd Khalid
Universiti Malaysia Terengganu
Erick Naim
Universiti Malaysia Terengganu
Riza Yuliratno Setiawan
Universitas Gadjah Mada
Edward J. Anthony
Aix-Marseille Universite

Research article

Keywords: Mangrove, Tidal channel meander, Mangrove geochemistry, Mangrove sedimentation

Posted Date: May 11th, 2020

DOI: https://doi.org/10.21203/rs.3.rs-27297/v1

Version of Record: A version of this preprint was published on September 7th, 2020. See the published version at https://doi.org/10.1186/s40645-020-00362-y.

Abstract

Tropical mangrove swamps are commonly characterized by dense networks of tidal channels that may show pronounced meandering and dendritic patterns. Channel meanders are sometimes accompanied by cut offs, and, like classical fluvial meanders, record changes in hydrology and sedimentation over time. Channel meandering can, thus, be an important process that contributes to spatial and temporal variability in the preserved record of the sedimentology and geochemistry of mangrove sediments. The aim of this study is to highlight changes in channel meander sedimentation in response to a meander cut-off in a tropical mangrove swamp. Two short sediment cores were sampled, respectively from a point bar (core KR1, 122 cm) at the junction with the neck cut-off and inside the cut-off (core KR2, 98 cm) in the Sungai Kerteh mangroves of Peninsular Malaysia. The profile comparison was based on sediment characteristics, total organic carbon (TOC) and selected elements (Fe, Na, Mg, Mn, Ba and Sr). Sedimentation rates at both sites were determined from 210Pb. A smaller standard deviation of mean grain size (MGS) was found at the point bar (4.37±0.51 ϕ) than in the cut-off (4.43 ±1.76 ϕ), indicating a difference in flow velocity between the two settings. A small difference in sedimentation rate between the upper (0.41 cm.yr-1) and bottom (0.50 cm.yr-1) parts of core KR1 suggests that water velocity at the point bar area has been rather uniform over the timescale of sedimentation. On the other hand, a higher sedimentation rate in the bottom (0.60 cm.yr-1), compared to the upper (0.39 cm.yr-1) part of core KR2 may reflect a reduction in sediment supply following cut-off. This change also resulted in increased accumulation of selected elements and TOC at the cut-off site from a depth of ~ 60 cm to the core-top segment probably associated with a slowing down of sediment settling. A higher TOC recorded in the cut-off (2.74±1.42%) compared to the point bar (1.14±0.46%) suggests a propensity for prolonged in-situ accumulation of organic matter in the abandoned meander bend. This study provides grain-size and sediment geochemical information that is consistent with patterns of long-term active and inactive sedimentation in the meander bends of mangrove channels.

Introduction

Tidal channels in mangroves are important pathways for the transport of sediments, dissolved oxygen, nutrients, seedlings and organic matter (Woodroffe, 1992; Anthony, 2009). Tidal network types and densities are highly variable, ranging from meandering to dendritic patterns, and, as noted by Allen (2000) for saltmarsh systems, they reflect several linked natural factors that are not well known, especially in comparison to the better known fluvial networks. One source of complexity is the bi-directional tidal flow, in comparison to the unidirectional flow in fluvial systems. As in the case of classical fluvial meanders (Leopold & Wolman, 1960; Ferguson, 1984; Howard, 2009), however, mangrove channel meanders are expected to record changes in channel hydrology and sedimentation over time. Meandering is formed by river flow momentum alternations from side to side within a channel, commonly across the floodplain, but the process is also inherent to shifting channels within a valley (Edwards & Smith, 2002). Meanders are dynamic systems that are far from equilibrium, driven by complex linear and nonlinear processes (Argyris et al., 1994). Theoretically, the flow erodes sediment at the outside of a bend as it reaches a

maximum velocity. The eroded materials are deposited as a point bar on the inside of the bend. These processes can lead to obstruction of flow at the neck, resulting eventually in the formation of a new shorter channel, a meander cut-off, and neck abandonment. Understanding these processes in mangrove forests can contribute to an understanding of changing present environments, under natural and human-induced processes that drive mangrove sedimentation, as well as of the paleo-environmental record (e.g., França et al., 2015; Cohen et al., 2016; Woodroffe et al., 2016). However, elucidation of these processes and the eventual messages that can be deduced regarding environmental changes can only be achieved through archives provided by sediment cores (e.g., Ellison & Stoddart, 1991; Ellison & Farnsworth, 1997). Such sedimentary archives provide a record of the type, rates, and patterns of sedimentation. Access to such information requires, however, both a classical sedimentological approach as well as geochemical characterization. Potential differences in sedimentation on meander convex banks and correlative erosion on meander concave banks have been evoked to explain differences in the vigour and health of mangroves that are generally clearly visible on aerial photographs and satellite images (Anthony, 2004). We know of no work, however, that has been undertaken to highlight the impact of channel meander evolution on mangrove sedimentation and on the sediment geochemistry. In this paper, we document changes in mangrove channel meander sedimentation associated with a meander cut-off in a Malaysian mangrove system (Fig. 1) using grain-size and geochemical characteristics of core sediments in the vicinity of an abandoned meander. We show that such sedimentological and geochemical characterization can be used in identifying change in mangrove environments.

Methods / Experimental

Study site

The mangroves of Sungai Kerteh are located in Kemaman District, Terengganu, Peninsular Malaysia (Fig. 1). The dominant mangroves are *Rhizophora apiculata* and *Avicennia sp*. A major morphological feature of the area is the Kerteh River, approximately short 23 km-long coastal river that originates in hilly terrain at ~ 600 m above sealevel, before running through the mangroves and reach the tidal channel at the east. The Kerteh receives runoff from a number of smaller tributaries at the upstream. The lower reaches of the Kerteh are influenced by semi-diurnal tides. The tidal range in the area is mesotidal, ranging from 0.2 m at low tide to 3.3 m at high tide during spring tides (PHN, 2019). There are no data on water discharge of the Kerteh River, which is modulated seasonally by Monsoon rainfall (mean annual: ~2800 mm) and at shorter timescales by the spring-neap tidal range.

The Kerteh River displays prominent meanders typical of mature mangrove swamps that are probably characterized by low substrate sedimentation rates, as suggested by the morphological stability of the channels. Locally, however, this stability has been affected or enhanced by embankments associated with villages and communities located on the channel banks. According to the classification by Jackson (1978), the present Kerteh channel can be considered as muddy fine-grained, with a low width/depth ratio, steep point bar slopes and prominent levees. The study site is a meander with a cut-off upstream of Kampung Gelugor (Fig. 1). Sediments were sampled at two different locations in the Kerteh mangroves

(Fig. 1): the neck cut-off (core KR1) and the inside of a meander (core KR2). The KR1 site is located at the confluence of two tidal channels, one of which included the cut-off reach with sampling site KR2. The dominant species at KR1 is *Rhizophora apiculata* whereas KR2 consists of mixed *Avicennia* sp. and *Rhizophora apiculata*.

Sampling and sample pre-treatment

The two cores were collected at low tide by driving a 2.5 m polyvinyl chlorice (PVC) tube with a diameter of 6.5 cm into the mangrove sediment. A tight cable and rope were attached to the middle part of the PVC tube in order to retrieve it from the mangrove. A cork and plastic were used to cover the top of the tube neatly to create a vacuum condition, enabling slow and cautious recovery of the cores. The pull-out process was conducted carefully to reduce loss of sample material and to maintain the lithological structure of the core sediment. Samples were taken from the cores in the laboratory for analysis of grain size, metal content, total organic carbon, and ^{210}Pb.

Sediment characteristics

Approximately 5 g of the sediment samples were transferred into a 100 ml beaker and diluted with distilled water as a medium for the digestion process. A few drops of hydrochloric acid (HCl) and 15% of hydrogen peroxide (H_2O_2) were added into the beaker to remove carbonate content and organic materials. Calgon solution (20% Sodium Thiosulphate) was added and acted as an agent to disperse the samples into single particles. The samples were left at room temperature for 24 hours to allow complete particle dispersion of particles. Sediment samples were analyzed using a laser diffraction analyzer (MALVERN Mastersizer 2000). All data collected were subjected to statistical analysis using the moments statistical method (Friedman & Johnson, 1982). The sediment grain-size characteristics (particle mean grain size and sorting) were calculated using the formula of Folk and Ward (1957). The relative proportions of sand, silt and clay were determined using the textural triangle proposed by USDA (1987).

Total organic carbon

The total organic carbon was determined based on the Walkley-Black chromic acid wet oxidation method (Walkley & Black, 1934; Allison & Moodie, 1965). Approximately 10 ml of potassium dichromate was added to 0.5 g of sample in a test tube. Then 20 ml of sulfuric acid was added and left in a beaker of boiling water (30 min). The test tube was rinsed with 200 ml of distilled water into a conical flask and 10 ml of phosphoric acid with a 1 ml Diphenylamine indicator added. The solution was mixed until it turned dark blue. Finally, Ferum (II) sulfate was titrated until the solution turned green and the total volume of Ferum (II) sulfate was recorded. The calculation of organic carbon content was as follows:

TOC (%) = (V1-V2) x 0.03 × 100 / sample weight (g)

where,

V1 = volume of potassium dichromate (ml)

V2 = volume of Ferum (II) sulfate (ml)

A blank sample was included in order to determine the background content of organic carbon while a glucose sample was used as a control. The standard value percentage of total organic carbon in glucose is approximately 36 ± 5%.

Metal analysis

Sample digestion followed the published methods of Noriki et al. (1980) and Kamaruzzaman (1999) with the modification of mixed acid ratio and digesting temperature. Approximately 0.05 g of homogenized samples were digested in a concentrated mixed acid ratio of HF, HNO_3 and HCl (2: 3.5: 3.5) in a sealed Teflon vessel at 100 °C for 7 hours. After cooling to room temperature, a clear digested solution was transferred into a 15 ml polypropylene test tube and diluted with deionized water. An inductively coupled plasma mass spectrometer (ICP-MS) was used for the precise determinations of selected heavy metals (Fe, Mg, Cu, Mn, Ba and Sr). The accuracy of the analytical procedure was assessed by analyzing standard research material in duplicate from the National Bureau of Standard (NBS) 1646a. The recovery test coincided with the certified values of NBS 1646a. The recovery percentage of measured metals was found to be acceptable, ranging between 86.99% and 109.50% (Table 1).

Table 1
The value of accuracy analysis for standard reference

Trace Element	Certified Value	Analysis Value	Percentage (%)
Fe (%)	2.01 ± 0.04	2.20 ± 0.10	109.5
Mg (%)	0.40 ± 0.01	0.39 ± 0.27	97.5
Mn (mg/kg)	234.5 ± 2.80	204.0 ± 17.7	86.99
Sr (mg/kg)	68	65.2	95.88

^{210} Pb analysis

The ^{210}Pb dating method is an ideal tracer for sediments deposited during the last 100–150 years (Blais et al., 1995; Bakar et al., 2011). This method is useful for determining sedimentation rates, especially in areas of active water flow, such as coastal, nearshore, estuarine and mangrove areas (Mohamed et al., 1996). Sediment samples (1 g of 125 µm) were placed in a glass beaker with a known amount of Pb carrier $Pb(NO_3)_2$. The samples were then digested in 20 ml of 8M HCl for 3 hours at 40˚C. The digested samples were left to cool at room temperature. A 47 µm size filtrate paper was used for drying and then rinsed with 20 ml of 1% of $HClO_4$. Samples were separated by using the cation exchange column Bio-Rad AG 50W x 4 (200–400 mesh). The radioactivity of ^{210}Bi produced from ^{210}Pb was counted by using a gross α/β counter (Tennelec model Series 5 XLB low background gas-flowing anti-coincidence alpha–beta counter) after 30 days of electro deposition (Mohamed et al., 1996).

The quality of the analytical procedure was determined using the certified IAEA-315 Radionuclides in Marine Sediment as reference material. Blank samples were also analyzed to ensure accuracy. The results showed that the concentrations of ^{210}Pb were well within the certified value of 30.1 Bq/kg and the measured value of 23.9 Bq/kg. Blank samples did not indicate any significant contamination for the studied elements. The natural logarithm of unsupported ^{210}Pb detected in core KR1 and KR2 (Fig. 7) was used to obtain the sedimentation rate value based on the constant initial concentration (CIC) model (Appleby, 2001; Mahmood et al., 2011a, b).

Principal components analysis and factor analysis

The main component was extracted using principal component analysis through the Eigen decomposition method. Factor analysis was used to explain the latent variables rendered in the data sets using the Varimax method after Kaiser normalization. Factor loading scores were categorized as follows: VF > 0.75 (strong), 0.75 < VF > 0.5 (moderate) and < 0.50 (weak), corresponding to the absolute varifactor values (Liu et al. 2003). The statistical data processing and analysis were generated by using the software Minitab version 17 (Minitab Inc., State College, USA).

Results

Particle mean size and sorting, and sediment facies

Figure 2a shows the mean grain size (MGS) of sediment against depth for cores KR1 and KR2. Values ranged from 3.47 ϕ – 5.92 ϕ for KR1 and 1.52 ϕ – 6.47 ϕ for KR2. The highest and lowest MGS values in KR1 were recorded at depths of 32 cm and 52 cm, respectively. For KR2, the highest and lowest values occurred at depths of 56 cm and 82 cm. The profile of MGS in KR2 showed a significant change at 60 cm depth. Figure 2b shows the sorting values of sediment in both cores. KR1 ranged between 0.44 (moderately sorted) and 2.61 (moderately well sorted). The values of KR2 were between 1.60 and 2.30 (moderately sorted and moderately well sorted). The average value in KR2 was 1.60 ± 2.34 Ø with the highest value at 66 cm (2.61 Ø) and the lowest at 0.44 Ø. In KR1, the mean was 0.44 ± 2.61 Ø with the highest value at a depth of 32 cm (2.34 Ø) and lowest value at 102 cm (1.60 Ø). The best-sorted sediment was recorded at a depth of 80 cm in core KR1. As in the case of MGS, sorting also showed the same trend with depth. Figure 3 shows a textural classification plot of sediment in the two cores. The sediments in KR1 from the point bar exhibit a high percentage of sand (40–80%) in contrast to sediment from KR2 from the meander cut-off which is less sandy (10–40%).

Total organic carbon

The TOC was determined in KR1 and KR2 (Fig. 2c). The TOC content was significantly higher in core KR2 ranging from 0.6% – 5.5% as compared to core KR1 with values of 0.24% – 4.26%. The average TOC values in core KR2 and KR1 were 2.74% ± 1.42% and 1.14% ± 0.46% (Fig. 2c). There were two obvious trends between TOC contents of cores KR1 and KR2. Like the metal and MGS trends, there were two

apparent trends for TOC content in both core samples. The TOC content fluctuated from the bottom of the core towards the surface with no significant changes for core KR1. On the other hand, the content in core KR2 was only comparable to that of core KR1 at depths between 98 cm and 76 cm. The concentration of TOC drastically increased at a depth of 72 cm and remained high up to the surface of the core.

Metals

The element concentrations in core KR1 varied from 0.32 to 2.18% (Fe), 0.51 to 2.38% (Na), 0.49 to 0.95% (Mg), 81.60 to 204.00 mg/kg (Mn), 22.40 to 47.60 mg/kg (Ba) and 1.37 to 7.98 mg/kg (Sr) (Fig. 4). The average concentrations of Fe, Na, Mg, Mn, Ba and Sr were 1.25 ± 0.30%, 1.21 ± 0.77%, 057.92 mg/kg, 63.01 ± 15.49 mg/kg, 17.48 ± 2.14 mg/kg and 9.1 ± 1.5 mg/kg. The element concentrations in core KR2 varied from 0.07 to 2.24% for Fe, 0.30 to 2.14% for Na, 0.01 to 0.71% for Mg, 5.34 to 173.80 mg/kg for Mn, 3.20 to 34.20 mg/kg for Ba and 0.50 to 6.52 mg/kg for Sr. The average concentrations of elements in this study followed the order of Fe > Na > Mg > Mn > Ba > Sr. In general, the selected element content in KR1 did not show an abrupt change from the bottom towards surface. However, the element content in the core KR2 showed a significant increase at a depth of ~ 70 cm.

^{210} Pb activity

Figure 5 shows the concentration of ^{210}Pb activity in each core. The concentrations in core KR1 varied between 21.03 Bq/kg (n = 14) and 50.37 Bq/kg (n = 14). In core KR2, ^{210}Pb activity concentrations varied between 18.55 Bq/kg (n = 12) and 48.63 Bq/kg (n = 12). ^{210}Pb activity concentrations in both cores fluctuated from the bottom toward the top of the core. Generally, the average activity concentrations in both cores were almost similar with values of 32.06 Bq/kg ± 10.85 Bq/kg and 30.41 Bq/kg ± 9.91 Bq/kg. The average sedimentation rates deduced from the concentrations was 0.46 cm.yr^{-1} at the point-bar location of core KR1 and 0.50 cm.yr^{-1} at the meander cut-off represented by KR 2 (Fig. 6).

Discussion

Cut-offs have been considered as having an important role in shaping river meander landscape by leading to the isolation of meander bends and perturbing the local dynamics (Hooke, 1977; Camporeale et al., 2008; Schwenk & Foufoula-Georgiou, 2016). In mangroves and saltmarshes, entrenched tidal channel networks are deemed to evolve very slowly through processes that include meander-bend erosion and sedimentation, with subsequently, very slow change of these inherited forms over multi-decadal to centennial timescales (Anthony, 2009). The ^{210}Pb activity, grain-size characteristics and selected aspects of the geochemistry of sediment cores in the vicinity of a mangrove tidal channel meander bend in Malaysia highlight an abrupt change in channel hydrodynamic and sedimentation regimes following a meander cut-off. Although there was no significant change in the average sedimentation rate between the point bar (KR1) and the cut-off (KR2), there was an obvious difference in sedimentation rates between the bottom and upper parts of the latter core. The sediment accumulation rate was relatively higher at the

bottom (0.60 cm.yr^{-1}) than the upper part (0.39 cm.yr^{-1}) of the sediment core. This indicates an abrupt reduction in sediment deposition rates in the top half of the core. A scrutiny of available aerial photographs and Google Earth images shows that the Kerteh cut-off has been extant over the last 13 years. The Kerteh displays a straight, nearly 1 km-long cut-off channel (Fig. 1) that points out to a rather abrupt hydrological change, rather than being the product of the slow progressive rapprochement of two opposite channel segments that eventually coalesce, forming a cut-off. The cut-off may well have occurred during the big flood event that hit Terengganu nearly a century ago from 21 to 29 December, 1926, accompanied by exceptional rainfall (1944 mm compared to the annual mean of ~ 2800 mm), and resulting in severe environmental damage and the destruction of thousand hectares of forests were destroyed (Chan, 2012; Williamson, 2016). However, this time frame largely exceeds a cut-off age of about 25–30 years estimated from sedimentation rates based on the ^{210}Pb activity (Fig. 7), if we assume such rates to be constant, which is manifestly not the case in the two cores where the sedimentation rates would have been influenced by physical, chemical, biological factor.

Whatever the true age of the cut-off, the change engendered by this event is also recorded in the grain-size and TOC trends. Sediment particle characteristics have been shown to provide information on the relationship between hydrodynamics and transport or deposition (e.g., Droppo, 2015). The dominantly fine-grained nature of the sediments found in KR1 and KR2, composed essentially of silts and, to a lesser degree, clays (Figs. 2, 3), reflects both the high degree of weathering of tropical soils and the effect of mangrove swamps on dampening water flows and favouring the accumulation of mud. Notwithstanding, differences in grain size have been found between the two cores in the Kerteh swamp. Core KR2 shows, in particular, a very sharp transition from coarse, through fine to medium sand, at a depth of about 80 cm, to relatively homogeneous silt and clay in the rest of the upper part of the core. We attribute this sharp change to the transition from an active channel meander to meander cut-off. Meander cut-offs in tidal environments have been shown to exhibit sharp upward changes in facies following abandonment (e.g., Anthony et al., 1996). The coarse basal deposits correspond to sand deposited in an active channel bed. Once the cut-off occurred, the diversion of flows through the straight new channel was accompanied by a slow-down in sedimentation rate characterized by a shift to fine-grained deposits associated with settling in a low-energy, abandoned channel environment. The sedimentation rate and grain size in KR1 are relatively more homogeneous, though the upper part of the core (above 70 cm) shows a clearly overall fining trend and a lower sedimentation rate. These characteristics reflect a slight shift from relatively more coarser-grained sedimentation at the base to more continuously finer-grained point-bar sedimentation. The differences between the two cores are less manifest in sorting, with the exception of basal sediments in the point bar which show poor sorting, probably reflecting mixing of sediment in an energetic channel environment. It may be surmised that the abrupt change in sorting in this core may pinpoint the time of the meander cut-off. Fleming (2017) identified a tendency for sorting to be homogeneous in sediment composed of a similar range of size, whereas poor sorting implies sediment mixing with different sizes of sediment.

The abrupt variation in grain-size and sedimentation rate in the meander cut-off is also consistent with an increase in OC, thus further reflecting the consequences of this event on local sedimentation. Both particle size distribution and OC concentrations changed significantly at ~ 70 cm, pointing to a change in the depositional environment. Meander cut-offs in tidal flats have been shown to be depocentres of organic matter following the instauration of quiescent hydrodynamic conditions, as flow becomes diverted through the cut-off (Anthony et al., 1996). This increase in OC has also been shown to go with a decrease in grain size (Sutherland, 1999). Generally, OC binds more easily with fine sediment, clay or silt.

Previous studies have shown that the distribution of heavy metals in sediment is closely related to organic matter and mostly depends on the type of sediment (Karbassi et al., 2005; Sabuti & Mohamed, 2013; Abdul Razak et al., 2018). The metal concentration in the point bar is almost uniform from the bottom to the top of the core, whereas the concentration in the cut-off shows a clear transition phase at a depth of 70 cm, thus further providing evidence for a morpho-sedimentary change in the Kerteh channel associated with meander cut-off. The abandonment of the meander created conditions for the active accumulation of elements and OC in the cut-off, compared to the point bar. Louma (1990) has shown this relationship between the concentration of elements and sedimentation processes. The variability in metal concentration has also been shown to depend on the size and texture of sediments (Jicknell and Kump 1984; Ramos et al., 1994), with larger mean grain size being associated with a larger variation of metal concentration at the same area (Morse et al., 1993).

In order to further clarify the relationships in the grain size and geochemistry of these deposits, we used a correlation coefficient matrix for each core (KR1: Table 2; KR2: Table 3). The correlation of metals with mean grain size and TOC in cut-off was relatively stronger compared to the point bar. The highest correlation value of the latter is 0.76 (Fe-Mg), followed by Fe-Cu (r = 0.75), Cu-Sr (r = 0.74), Mg-Mn (r = 0.73), Mean Sediment-TOC (r = 0.71) and TOC-Fe (r = 0.71). The highest correlation value of the cut-off is r = 0.98 (Mg-Mn), whereas the lowest correlations occur between Ba-Fe (r = 0.59) and Ba-TOC (r = 0.53), although both are still considered as strongly correlated to each other. The strong positive correlation between all parameters in the cut-off suggests that grain size is an important criterion for the attachment of metals and TOC under the conditions of reduced flow energy that ensued following meander abandonment. Nguyen et al. (2005) have shown that highly correlated metals exhibited a similar behavior in the study area. Generally, the contents decreased as grain size increased.

Table 2
Correlation coefficient between MGS, TOC and selected metals in core KR1.

	MGS	*TOC*	*Fe*	*Na*	*Mg*	*Mn*	*Ba*	*Sr*
MGS	1							
TOC	0.71	1						
Fe	0.60	0.71	1					
Na	0.30	0.30	0.59	1				
Mg	0.46	0.50	**0.76**^{H}	0.58	1			
Mn	**0.18**^{L}	0.20	0.48	0.41	0.73	1		
Ba	0.27	0.36	0.53	0.40	0.78	0.56	1	
Sr	0.24	0.15	0.42	0.41	0.74	0.56	0.59	1
*note: H: Highest correlation; L: Lowest correlation								

Table 3
Correlation coefficient between MGS, TOC and selected metals in core KR2.

	MGS	*TOC*	*Fe*	*Na*	*Mg*	*Mn*	*Ba*	*Sr*
MGS	1							
TOC	0.89	1						
Fe	0.92	0.94	1					
Na	0.88	0.88	0.89	1				
Mg	0.92	0.86	0.91	0.89	1			
Mn	0.89	0.83	0.89	0.84	**0.98**^{H}	1		
Ba	0.66	**0.53**^{L}	0.59	0.68	0.83	0.81	1	
Sr	0.74	0.63	0.66	0.72	0.86	0.85	0.90	1
*note: H: Highest correlation; L: Lowest correlation								

Principal components analysis (PCA) highlighted two significant compounds (eigenvalue > 1) that explained 71.2% (KR1) and 93.0% (KR2) of the total variance of the datasets (Table 4). For KR1, varifactor VF1 explained 28.3% of the total variance in the datasets with positive loadings on metal content such as Mg (0.89), Mn (0.79), Ba (0.75), and Sr (0.86). Varifactor VF2 accounted for 32.8% of the total variance with positive loadings on mean grain size (0.75) and total organic content (0.90). Meanwhile, for KR2,

varifactor VF1 explained 54.7% of the total variance with strong loadings on MGS (0.83), total organic carbon (0.90) and metal, namely Fe (0.90) and Na (0.80), whereas varifactor VF2 accounted for 38.3% with negative loadings exhibited by the concentrations of Ba and Sr. The PCA shows that only Fe and Na are influenced by changes in MGS and organic content. In this study, communalities of the variance explained a higher value for KR2 (0.88–0.97) than KR1 (0.50–0.93), revealing that the extracted factor fitted well with factor solution.

Table 4
Varifactors of varimax rotated loading results

Variable	KR1			KR2		
	VF1	VF2	Communality	VF1	VF2	Communality
Depth	-0.07	-0.82	0.68	-0.91	0.23	0.88
MGS	0.18	0.75	0.60	0.83	-0.48	0.92
TOC	0.14	0.90	0.84	0.90	-0.32	0.92
Fe	0.54	0.71	0.81	0.90	-0.38	0.96
Na	0.58	0.34	0.50	0.80	-0.49	0.88
Mg	0.89	0.37	0.93	0.69	-0.69	0.97
Mn	0.79	0.09	0.64	0.65	-0.70	0.93
Ba	0.75	0.30	0.66	0.25	-0.93	0.94
Sr	0.86	-0.05	0.75	0.36	-0.89	0.93
% Variance	38.3	32.8		54.7	38.3	

It is noteworthy that a distribution pattern of metal content versus sample depth was clearly observed in KR2 (Fig. 7b) compared to KR1 (Fig. 7a). Two clusters were formed in KR2 in which metal accumulation in the upper depths had a higher concentration. The relationship between metal (Fe, Na) and MGS or organic content was much stronger for KR2 than KR1. This was highlighted by a straight line with a similar direction on the biplot graph (not shown). We deduce from this the relationship that the accumulation of finer-grained sediments following meander cut-off is favourable to binding between metals and organic matter.

The long-term (multi-decadal) mobility of mangrove tidal channels has been shown to depend essentially on sediment inputs into the system, which alter the morphodynamics of meanders, thus eventually generating, over even longer timescales (secular to millennial) the gradual reworking of mangrove tidal flats (Anthony, 2004). Active meander belt reworking in mangrove swamps occurs where high sediment loads in channels, notably bedload, induces instability in flow conditions. This has probably the case in the Kerteh tidal channel, given the ‘abrupt’ morphology of the meander cut-off (Fig. 1). The foregoing study of sediments associated with the tidal channel in the Kerteh Sungai mangrove swamp has shown

that channel dynamics can be important in generating variability in the sedimentology and geochemistry of mangrove sediments. The reasons for the formation of a meander cut-off in this swamp are not clear. However, since its formation, the Kerteh channel and its meander cut-off have exhibited apparent stability at the timescale of available satellite images and aerial photographs covering the study area (13 years). This stability suggests that the swamp and its channel network may now be largely in equilibrium with flow conditions.

Conclusions

This study has shown that geomorphic changes in mangrove tidal channels can generate significant variations in sediment characteristics and geochemistry. The data from two cores in contrasting local geomorphic situations associated with channel meandering show clear trends in metal concentrations, MGS and sorting, and TOC. The most noteworthy aspect highlighted by the study is that abrupt changes in channel flow conditions generated by a meander cut-off can induce marked changes in the sedimentology and geochemistry of sediments over time. Spatio-temporal changes in the dynamics of tidal channels in mangrove swamps are, thus, an important mechanism in generating variability in the long-term sedimentology and geochemistry of mangrove sediments.

Abbreviations

CMB: Core-mantle boundary; GOSAT: Greenhouse Gases Observing Satellite; IAEA: International Atomic Energy Agency; MGS: mean grain size; ICP-MS: inductively coupled plasma mass spectrometer; JAXA: Japan Aerospace eXploration Agency; NBS: National Bureau of Standard; TRMM: Tropical rainfall measuring mission; USDA: United States Department of Agriculture.

Declarations

Availability of data and material

The datasets used and/or analysed during the current study are available from the corresponding author on reasonable request.

Competing interests

The authors declare that they have no competing interest.

Funding

This work was supported by the Research Acculturation Grant Scheme (RAGS) [Vot. 57097, 2013].

Authors' contributions

Shaari H. conceived of the presented idea, developed the theory, performed the computations, verified the analytical methods and in charge of overall direction and planning. He also encouraged Nasir Q.M. and Naim E. to investigate the geochemical compounds and supervised them in order to accomplish the findings of this work.

Nasir Q.M. carried out the experiment, wrote the manuscript with supporting idea from Hasrizal Shaari.

Mohamed C.A.R. carried out the experiment of the Pb210 analysis in his laboratory at Universiti Kebangsaan Malaysia.

Yusoff A.H. helped interpretation of ^{210}Pb activity and wrote the discussion of sedimentation rate in the study area.

Khalid W.M.A.W.M. provided the statistical analysis of data and carried out the calculations.

Naim E. carried out the experiment, wrote the manuscript with support from Hasrizal Shaari.

Setiawan R.Y. provided critical feedback and helped shape the research, analysis and manuscript.

Anthony E.J. contributed on conceptual ideas and proof outline. He verified the data and wrote the important part of the discussion with input from all authors.

Acknowledgements

This work was supported by the Research Acculturation Grant Scheme (RAGS) [Vot. 57097, 2013]. The author would like to thank Mr. Syed Shahrul Afzan Syed Bidin, staff of Faculty of Science and Marine Environment, and Institute of Oceanography and Environment (INOS), Universiti Malaysia Terengganu for their assistance in this project.

References

1. Abdul Razak NS, Shaari H, Husain ML, Minhat FI, Mohd Azmi MF (2018) Vertical profile of heavy metals in mangrove and lagoon sediment cores of Sungai Kilim, Langkawi, Malaysia. Poll Res 37(1):41–50
2. Allen JRL (2000) Morphodynamics of Holocene salt marshes: a review sketch from the Atlantic and Southern North Sea coasts of Europe. Quat Sci Rev 19:1155–1231. doi:10.1016/S0277-3791(99)00034-7
3. Allison LE, Moodie CD (1965) Carbonate in methods of soil analysis. In: Black CA (ed) Chemical and Microbiological Properties. Soc. Agron. Inc. Madison, Wisconsin, pp 1387–1388
4. Anthony EJ (2004) Sediment dynamics and morphological stability of an estuarine mangrove complex: Sherbro Bay, West Africa. Mar Geol 208:207–224. doi:10.1016/j.margeo.2004.04.009

5. Anthony EJ (2009) Shore processes and their palaeoenvironmental applications: Chap. 3: tidal flats. Developments in Marine Geology Volume 4. Elsevier, Amsterdam, p 519
6. Anthony EJ, Lang J, Oyédé LM (1996) Sedimentation in a tropical, microtidal, wave-dominated coastal-plain estuary. Sedimentology 43:665–675. doi:10.1111/j.1365-3091.1996.tb02019.x
7. Appleby PG (2001) Chronostratigraphic techniques in recent sediments. In: Last WM, Smol JP (eds) Tracking Environmental Change Using Lake Sediments: Basin Analysis, Coring, and Chronological Techniques. Springer, Dordrecht, pp 171–203
8. Argyris J, Faust G, Haase M (1994) An exploration of chaos. An introduction for natural scientists and engineers. Texts Computer Mechanic 7, Elsevier, New York, p 751
9. Bakar ZA, Saat A, Hamzah Z, Wood K, Ahmad Z (2011) Sedimentation rate and chronology of As and Zn in sediment of a Recent former tin mining lake estimated using Pb-210 dating technique. Malay J Anal Sci 15(2):150–158
10. Blais MJ, Kalff J, Cornett RJ, Evans RD (1995) Evaluation of ^{210}Pb dating in lake sediments using stable Pb, Ambrosia pollen, and ^{137}Cs. J Paleolimnol 13:169–178. doi:10.1007/BF00678105
11. Camporeale C, Perucca E, Ridolfi L (2008) Significance of cutoff in meandering river dynamics. J Geophys Res 113(F01001):1–11. doi:10.1029/2006JF000694
12. Chan NW (2012) Impacts of disasters and disasters risk management in Malaysia: the case of Floods. In: Sawada Y, Oum S (ed), Economic and Welfare Impacts of Disasters in East Asia and Policy Responses. ERIA Research Project Report 2011-8, Jakarta, p 503–551
13. Cohen MCL, Lara RJ, Cuevas E, Oliveras EM, da Silveira SL (2016) Effects of sea-level rise and climatic changes on mangroves from southwestern littoral of Puerto Rico during the middle and late Holocene. Catena 143:187–200. doi:10.1016/j.catena.2016.03.041
14. Droppo IG, D'Andrea L, Krishnappan BG, Jaskot C, Trapp B, Basuvaraj M, Liss SN (2015) Fine-sediment dynamics: towards an improved understanding of sediment erosion and transport. J Soils Sed 15(2):467–479. doi:10.1007/s11368-014-1004-3
15. Edwards BF, Smith DH (2002) River meandering dynamics. Physic Rev E 65:46303. doi:10.1103/PhysRevE.65.046303
16. Ellison J, Stoddart D (1991) Mangrove ecosystem collapse during predicted sea level rise: Holocene analogues and implications. J Coast Res 7:151–165
17. Ellison AM, Farnsworth EJ (1997) Simulated sea level change alters anatomy, physiology, growth, and reproduction of red mangrove (*Rhizophora mangle L.*). Oecologia 112:435–446. doi:10.1007/s004420050330
18. Ferguson RI (1984) The threshold between meandering and braiding. In: Smith KVH (ed) Channels and Channel Control Structures. Springer, Berlin, pp 90–125
19. Fleming BW (2017) Particle shape-controlled sorting and transport behavior of mixed siliciclastic/bioclastic sediments in a mesotidal lagoon, South Africa. Geo-Marine Let 37:397–410. doi:10.1007/s00367-016-0457-3

20. França MC, Alves ICC, Castro DF, Cohen MC, Rossetti DF, Pessenda LCR, Lorente FL, Fontes NA, Junior AÁB, Giannin PCF, Francisquini MI (2015) A multi-proxy evidence for the transition from estuarine mangroves to deltaic freshwater marshes, Southeastern Brazil, due to climatic and sea-level changes during the late Holocene. Catena 128:155–166. doi:10.1016/j.catena.2015.02.005
21. Friedman GM, Johnson KG (1982) Exercises in sedimentology. Wiley, New York
22. Folk RL, Ward WC (1957) Brazos River Bar: A study in the significance of grain size parameters. J Sedimentol Petrol 27:3–26. doi:10.1306/74D70646-2B21-11D7-8648000102C1865D
23. Hooke JM (1977) The distribution and nature of changes in river channel patterns: the example of Devon. In: Gregory KJ (ed) River Channel Changes. Wiley, New York, pp 265–280
24. Howard AD (2009) How to make a meandering river. Proc Natl Acad Sci USA 106(41):17245–17246. doi:10.1073/pnas.0910005106
25. Jackson RG (1978) Preliminary evaluation of lithofacies models for meandering alluvial streams. In: Miall AD (ed) Fluvial Sedimentology. Canadian Society Petroleum Geologist Memoir 5, p 543–576
26. Leopold LB, Wolman MG (1960) River Meanders. Geol Soc Am Bull 6:769–793
27. Liu CW, Lin KH, Kuo YM (2003) Application of factor analysis in the assessment of groundwater quality in a blackfoot disease area in Taiwan. Sci Tot Environ 313(1–3):77–89. doi:10.1016/S0048-9697(02)00683-6
28. Louma SN (1990) Processes affecting metal concentrations in estuarine and coastal marine sediments. In: Furness RW, Rainbow PS (eds) Heavy Metals in the Marine Environment. CRC Press, Florida, pp 51–56
29. Nguyen HL, Leemakers M, Elskens M, Ridder FD, Doan TH, Baeyens W (2005) Correlation, partitioning and bioaccumulation of heavy metals between different compartments of Lake Balaton. Sci Tot Environ 341:211–226. doi:10.1016/j.scitotenv.2004.09.019
30. Kamaruzzaman BY (1999) Geochemistry or the Marine Sediments. Its Paleoceanographic Significance. Ph.D. Thesis, Hokkaido University, Hokkaido, unpublished
31. Jicknells TD, Kump AH (1984) The distribution and geochemistry of some trace metals in the Bermuda coastal environment. Estuar Coast Shelf Sci 18:245–262. doi:10.1016/0272-7714(84)90070-2
32. Karbassi AR, Nabi-Bidhend GhR, Bayati I (2005) Environmental geochemistry of heavy metals in sediment core off Bushehr, Persian Gulf. Iran J Environ Health Sci Eng 2:255–260
33. Mahmood ZUW, Mohamed CAR, Ishak AK, Bakar NSA, Ishak K (2011a) Vertical distribution of ^{210}Pb and ^{226}Ra and their activity ratio in marine sediment core of the East Malaysia coastal waters. J Radioanalytic Nuc Chem 289:953–959. doi:10.1007/s10967-011-1206-8
34. Mahmood ZUW, Mohamed CAR, Ahmad Z, Ishak AK (2011b) Intercomparison of techniques for estimation of sedimentation rate in the Sabah and Sarawak coastal waters. J Radioanalytic Nuc Chem 287:255–260. doi:10.1007/s10967-010-0672-8

35. Mohamed CAR, Narita H, Harada K, Tsunogai S (1996) Sedimentation of natural radionuclides on the seabed across the northern North Pacific. Geochem J 30:217–229. doi:10.2343/geochemj.30.217
36. Morse JW, Presley BJ, Taylor RJ, Benoit G, Santschi P (1993) Trace metal chemistry of Galveston Bay: water, sediments and biota. Mar Environ Res 36:1–37. doi:10.1016/0141-1136(93)90087-G
37. Noriki SK, Nakanishi T, Fukawa M, Uematsu T, Uchida H, Tsunogai S (1980) Use of a teflon vessel for the decomposition followed by determination of chemical constituents of various marine samples. Bull Fac Fish Hokkaido Univ 31:354–465
38. Pusat Hidrografi Nasional (PHN) (2019) Jadual pasang surut Malaysia 2019
39. Ramos L, Hernandez LM, Gonzalez MJ (1994) Sequential fractionation of copper, lead, cadmium and zinc in soils from or near Donana National Park. J Environ Qual 23:50–57. doi:10.2134/jeq1994.00472425002300010009x
40. Sabuti AA, Mohamed CAR (2013) Residence time of Pb-210, Bi-210 and Po-210 in the atmosphere around a coal-fired power plant, Kapar, Selangor, Malaysia. Poll Res 32(4):907–915
41. Schwenk J, Foufoula-Georgiou E (2016) Cutoffs accelerate nonlocal morphodynamic change. Geophys Res Let 43(12):437 –437 12,445. doi:10.1002/2016GL071670
42. Sutherland RA (1999) Distribution of organic carbon in bed sediments of Manoa Stream, Oahu, Hawaii. Earth Surf Process Landf 24:571–583. doi:10.1002/(SICI)1096-9837(199907)24:7%3C571::AID-ESP975%3E3.0.CO;2-F
43. U.S. Department of Agriculture (USDA) (1987) Agricultural resources: cropland, water and conservation situation and outlook report. AR-Economy Research Service, Washington, D.C.
44. Walkley A, Black IA (1934) An examination of Degtjareff method for determining soil organic matter, and proposed modification of the chromic acid tritation method. Soil Sci 37:29–38. doi:10.1097/00010694-193401000-00003
45. Williamson F (2016) The “Great Flood” of 1926: environmental change and post-disaster management in British Malaya. Ecosys Health Sustain 2(11):e01248. doi:10.1002/ehs2.1248
46. Woodroffe C (1992) Mangrove sediments and geomorphology. In: Robertson AI, Alongi DM (eds) Tropical Mangrove Ecosystem. American Geophysical Union, Washington D.C., pp 7–41. doi:10.1029/CE041p0007
47. Woodroffe CD, Rogers K, McKee KL, Lovelock CE, Mendelssohn IA, Saintilan N (2016) Mangrove sedimentation and response to relative sea-level rise. Ann Rev Mar Sci 8:243–266. doi:10.1146/annurev-marine-122414-034025

Figures

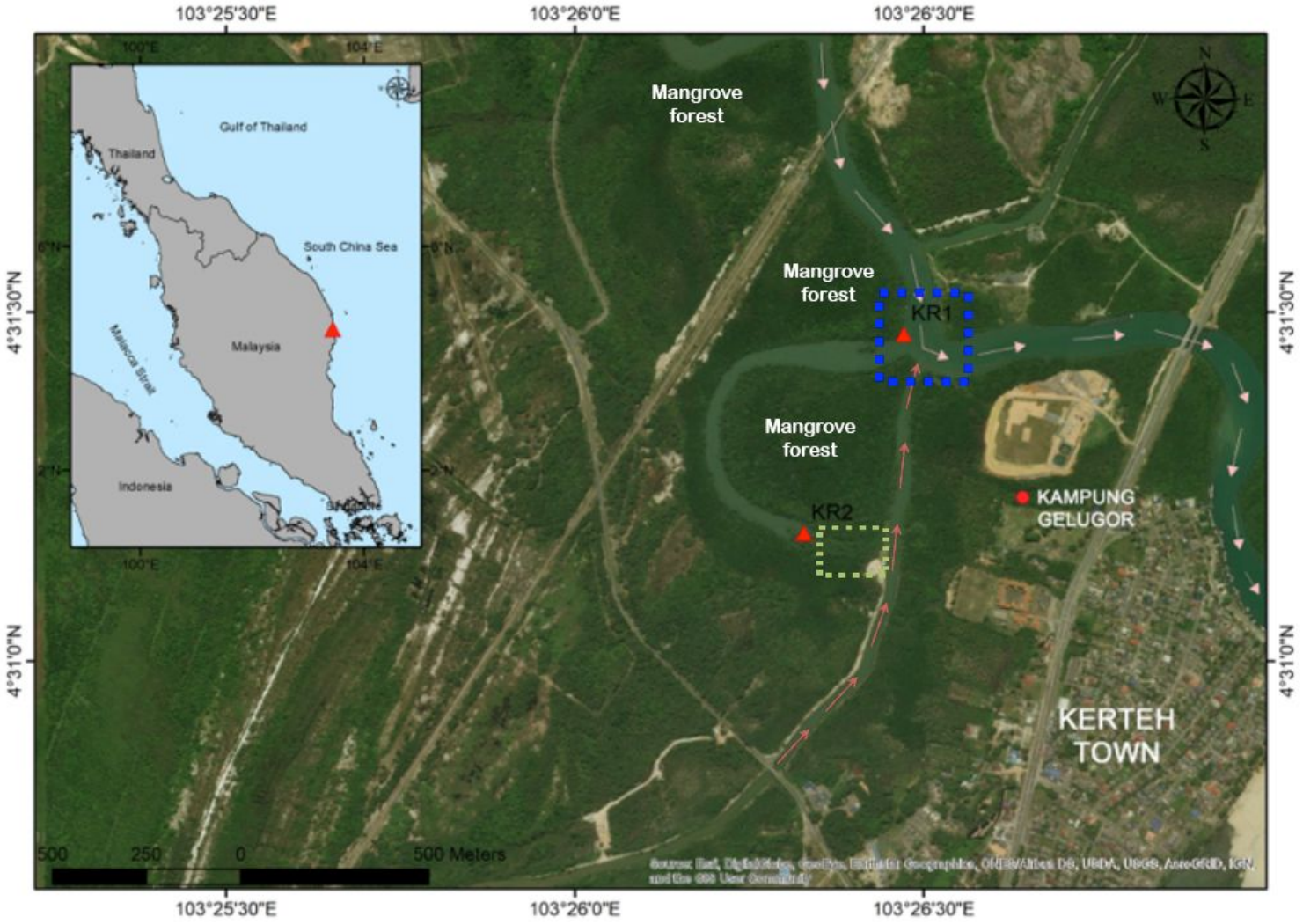

Figure 1

Map showing the Kerteh mangrove forest in Malaysia and the locations of cores KR1 (4°31'27. 5"N, 103°26'25.91"E) and KR2 (4°31'10.98"N, 103°26'19.68"E). The pink arrows indicate the river flow directions of main water body of Sungai Kerteh from upstream towards tidal channel and red arrows indicate the river flow direction from small branch of Sungai Kerteh. The blue dash box indicates the cutoff location and the pale green dash box indicates new mangrove vegetation at the old river's pathway due to the active sedimentation process. (source: Google Earth).

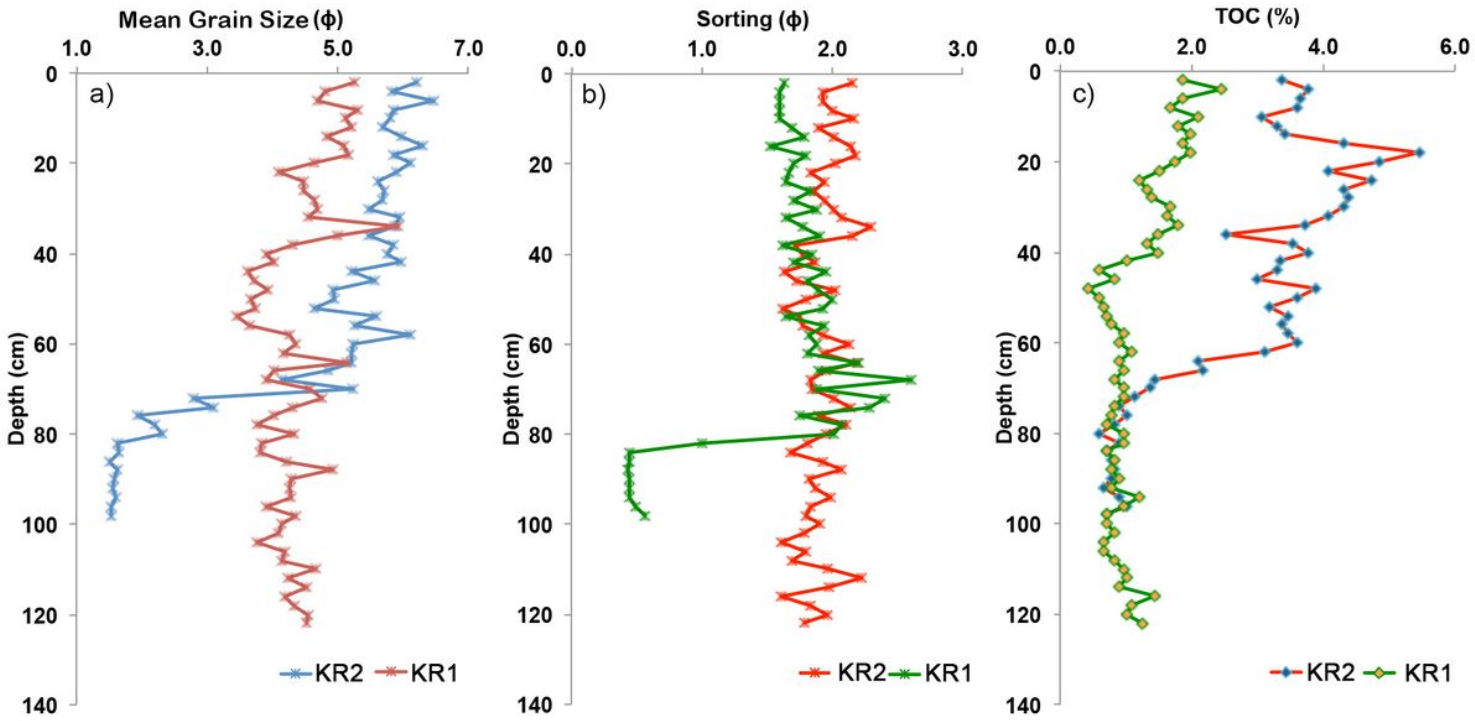

Figure 2

Vertical profile of: (a) mean grain size, (b) sorting, and (c) TOC.

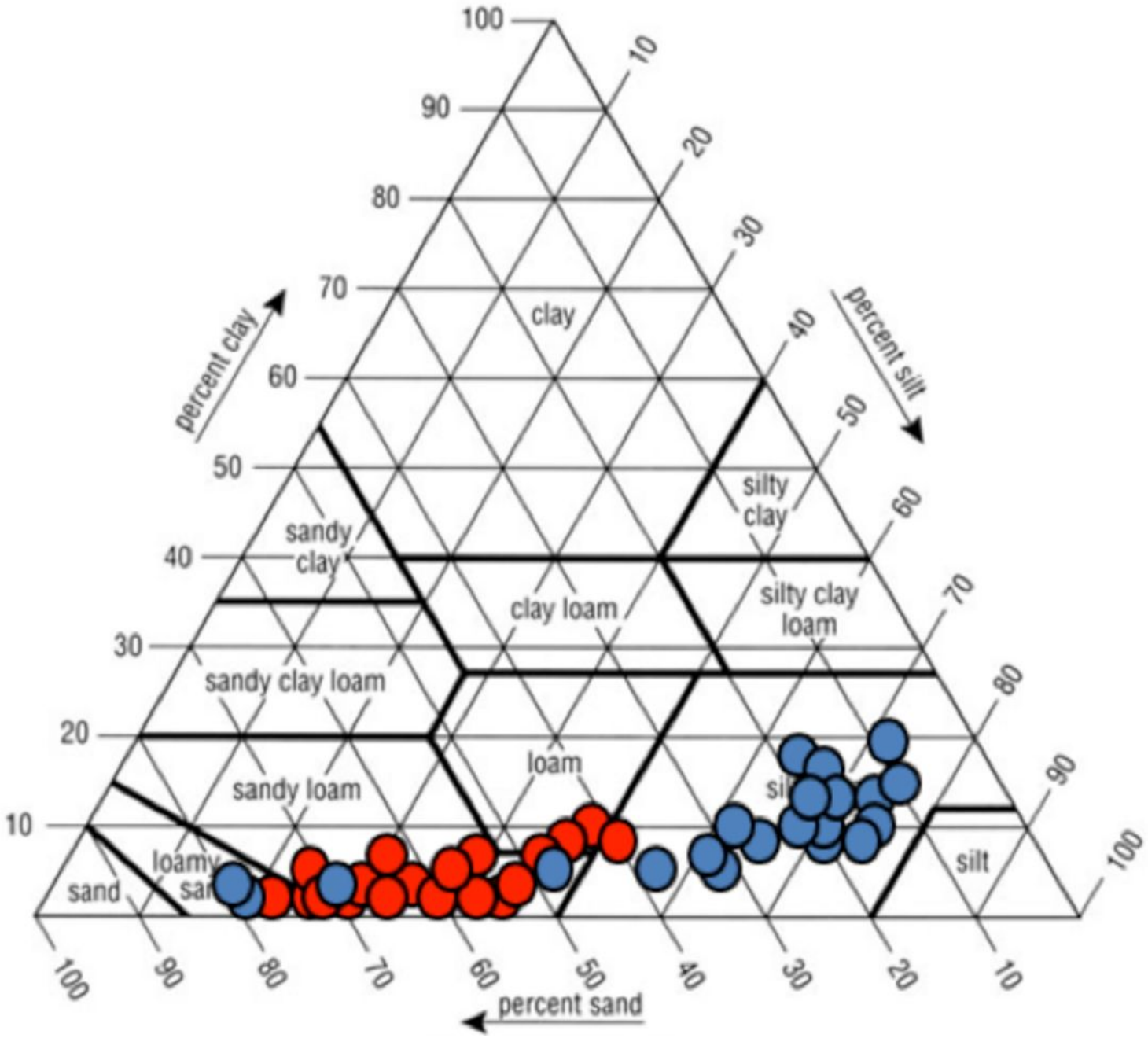

Figure 3

Textural classification of sediment from KR1 (red dots) and KR2 (blue dots)

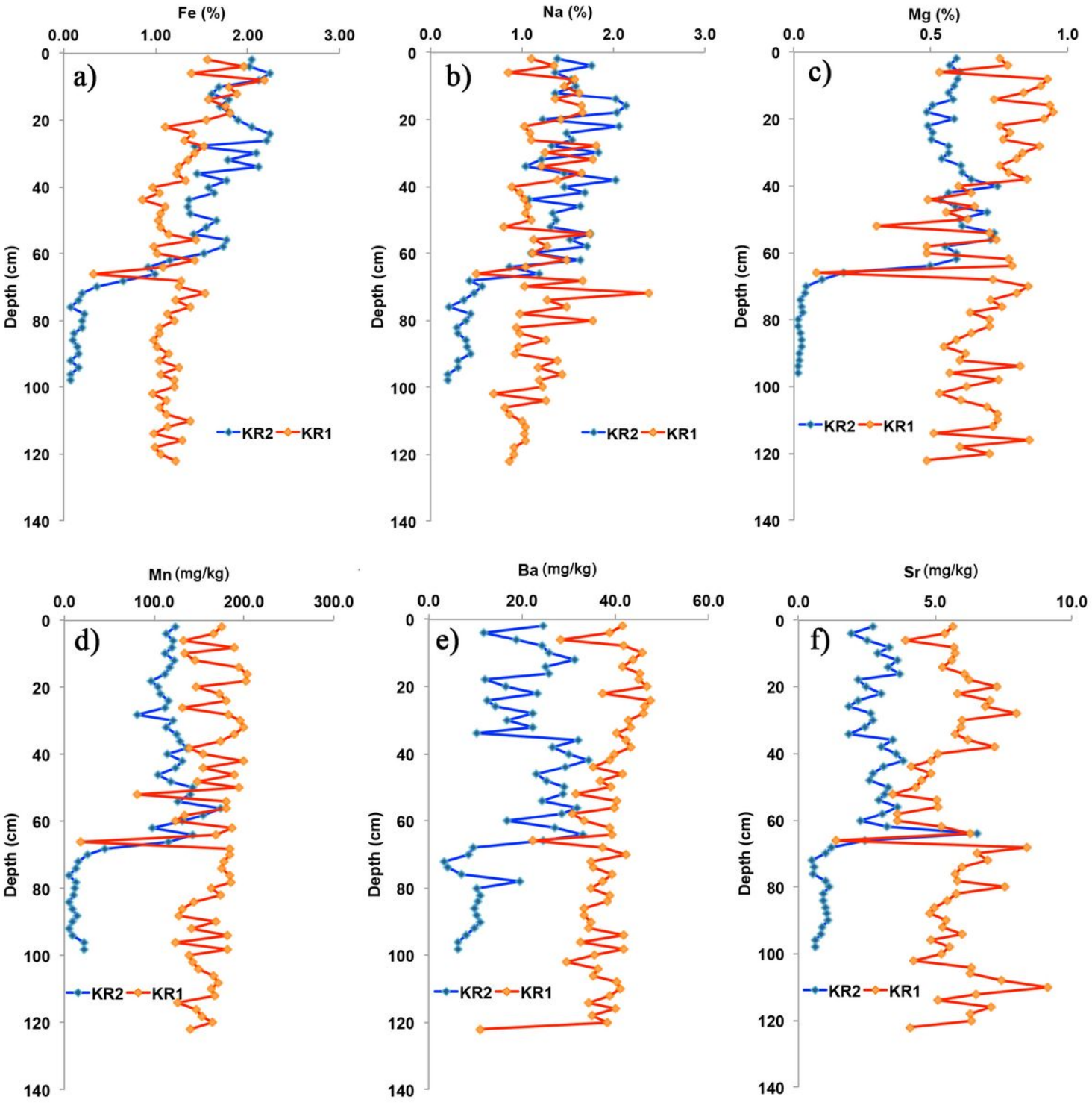

Figure 4

Selected metals concentrations in cores KR1 and KR2.

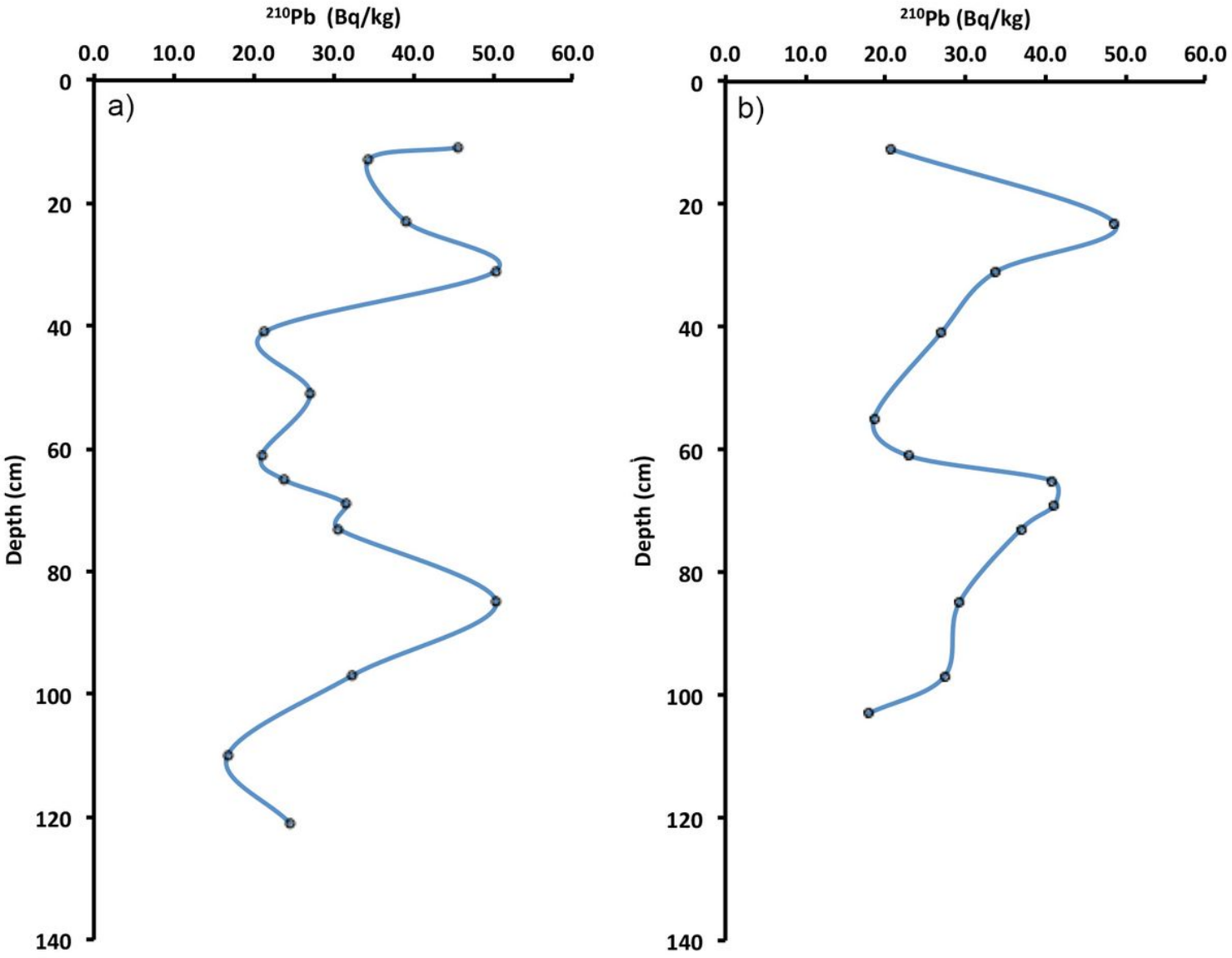

Figure 5

Concentrations of 210Pb activities in cores KR1 (a), and KR2 (b).

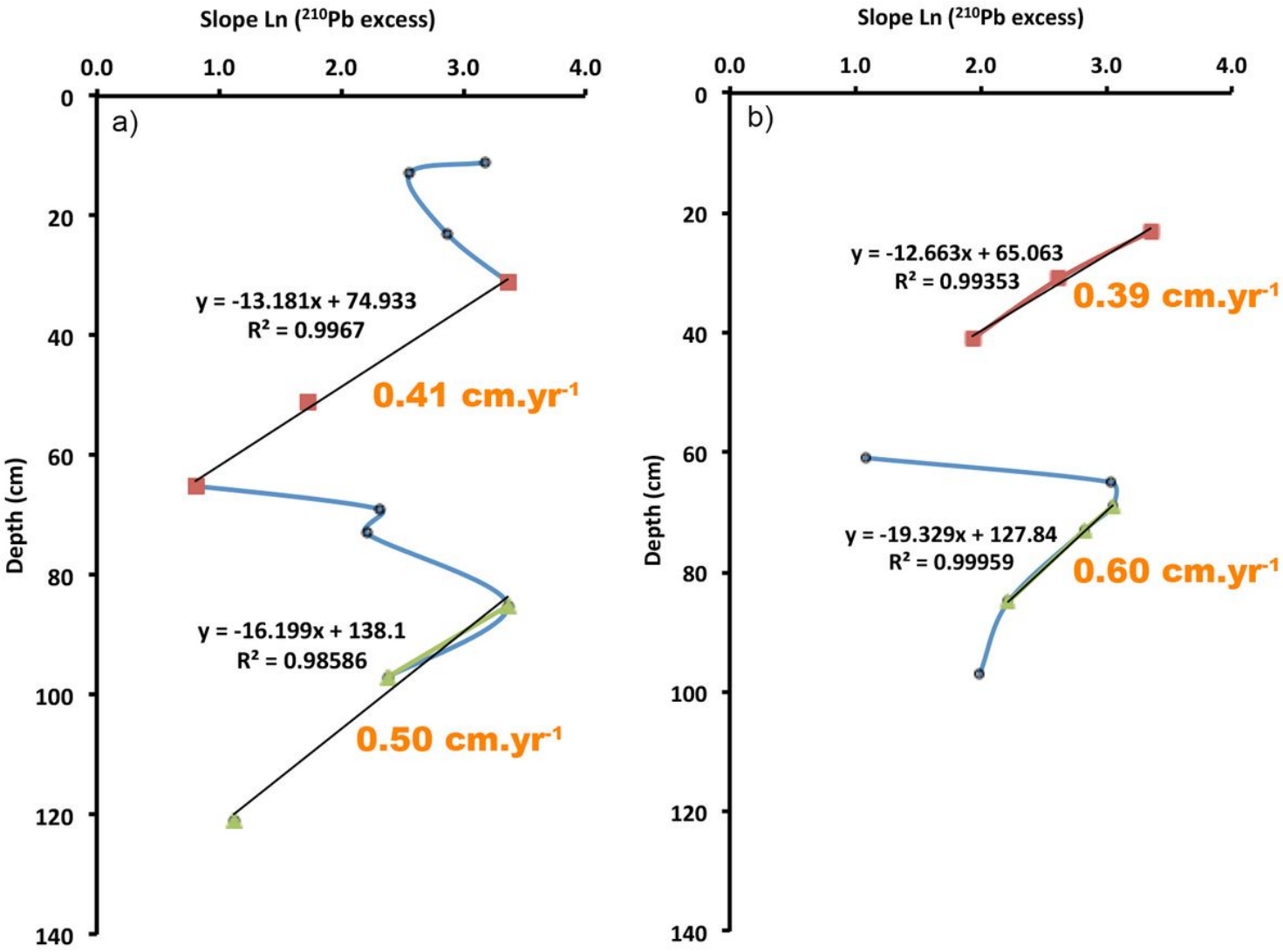

Figure 6

Graph Ln of 210Pb excess slope representing the sedimentation rates in cores KR1 (a) and KR2 (b).

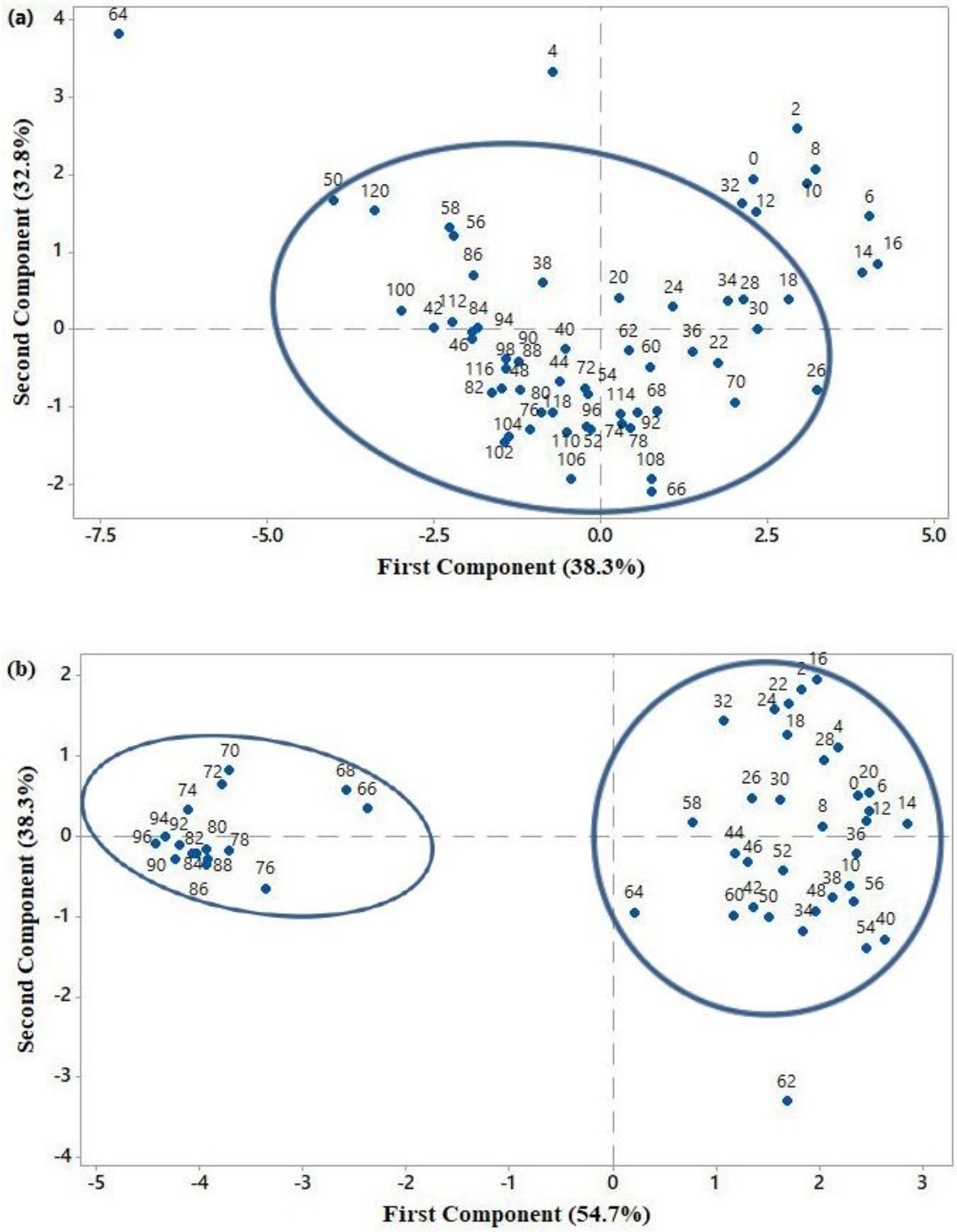

Figure 7

Loading plot of selected metals concentrations vs depth on KR1(a) and KR2 (b).

Supplementary Files

This is a list of supplementary files associated with this preprint. Click to download.

- GraphicAbstractImage.jpg